

Quantum Computing Gate Emulation Using CMOS Oscillatory Cellular Neural Networks

Richelle L. Smith, *Member, IEEE*, and Thomas H. Lee, *Fellow, IEEE*

Abstract—This paper presents quantum computing gate emulation using polychronous oscillatory cellular neural networks. The oscillatory neural network consists of locally interacting ring oscillators and control switches, in a standard CMOS process. We apply impulse sensitivity function (ISF) theory to model the injection locking of the oscillators. We show the design of universal quantum gate emulation with oscillator circuits. Quantum circuits for the Greenberger–Horne–Zeilinger State and W State are emulated using CMOS oscillators and switches. Spectre simulation results agree with the quantum circuit theory.

Index Terms—CMOS, cellular neural network (CNN), computing, neuromorphic computing, polychronization.

I. INTRODUCTION

QUANTUM computing and brain-inspired systems are promising alternatives to traditional von Neumann computing [1]–[10]. Quantum neuromorphic computing is an emerging field that combines quantum computation with neural networks [11]. Cellular neural networks (CNN), which are a neuromorphic architecture inspired by biological retinas [12]–[14], are a compelling approach for implementing brain-inspired systems. The CNN performs computations in continuous time, utilizing the physical dynamics of the circuit.

Recently, CMOS polychronous oscillatory cellular neural networks have been proposed, for solving graph coloring problems [15]. This approach combines CNNs [12]–[14] with coupled-oscillator based computing [16]. That is, each cell of the CNN is implemented as a CMOS oscillator with local connections to neighboring oscillators. The integrated CMOS oscillator approach provides the benefits of compact area and compatibility with standard foundries, leveraging existing infrastructure for design and manufacturing.

While cellular neural networks comprise a large body of research, the use of cellular neural networks to emulate quantum computing operations remains unexplored. Conventional quantum computers are bulky and require elaborate cooling systems, limiting their portability and widespread adoption. In the near term, quantum computing emulation has the potential to be an energy-efficient computing scheme that is suitable for room temperature and mobile applications.

In this brief, we propose quantum computing gate emulation using polychronous oscillatory cellular neural networks, shown in Fig. 1. In Section II, we briefly review the fundamentals of quantum computing gate emulation and propose to use polychronous oscillatory CNN. In Section III, we demonstrate how to emulate universal quantum gates using an

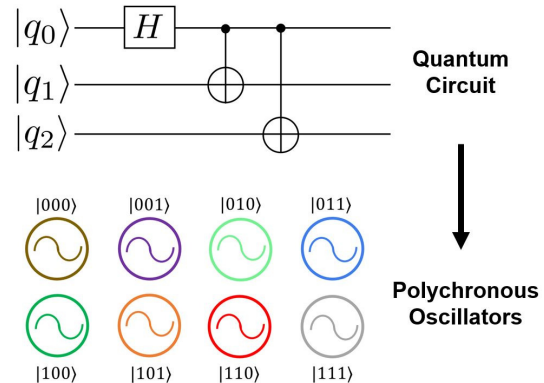


Fig. 1. Mapping of quantum circuit to polychronous oscillatory cellular neural network.

oscillatory CNN with CMOS ring oscillators and switches. In Section IV, we present CMOS circuit design of a polychronous oscillatory CNN for quantum gate emulation and examples of the Greenberger-Horne-Zeilinger State and W State, with simulation results.

II. QUANTUM COMPUTING GATE EMULATION USING A NETWORK OF POLYCHRONOUS OSCILLATORS

In this section, we first review the fundamentals of quantum computing gate emulation based on LC resonators. We then extend and generalize the theory, and propose to use polychronous oscillatory CNN.

A. Quantum Computing Gate Emulation Using LC Resonators

Mapping quantum gates to coupled LC resonators was proposed in [17], and extended by [18] to develop a circuit-simulation-based framework for quantum computing emulation. In these approaches, N qubits can be mapped to 2^N resonators. The probability of each quantum state is encoded in the amplitude of the voltage swing across the resonator. If a resonator has no voltage swing across it (is not oscillating), then the quantum state represented by the resonator has zero probability. For example, a two-qubit system can be represented by four resonators. The first resonator represents $|00\rangle$, the second resonator represents $|01\rangle$, the third resonator represents $|10\rangle$, and the fourth resonator represents $|11\rangle$.

However, the approaches in [17] and [18] involve time-varying inductances for the mixing gate and controlled NOT gate, and time-varying capacitance for the phase-shift gate and controlled phase-shift gate. Controlling a time-varying inductance with a precisely defined inductance as a function of time is challenging to implement in hardware. Besides, an array of LC oscillators is difficult to implement on chip due to the large area of planar inductors, and this limits the size of the array. Further, practical LC resonators have finite Q -factor and nonzero resistance, which dampens oscillation waveforms. Without a power source, oscillations die out over time.

Manuscript received 30 January 2024; revised xx April 2024. The work of Richelle L. Smith was supported by the ARCS Foundation Northern California Fellowship (William K. Bowes, Jr. Foundation Scholar).

Richelle L. Smith and Thomas H. Lee are with the Department of Electrical Engineering, Stanford University, Stanford, CA 94305 USA (e-mail: smithrl@stanford.edu and tomlee@ee.stanford.edu).

B. Proposed Approach: Polychronous Oscillatory CNN

To overcome the challenges of implementing an array of LC resonators with precise time-varying inductance and capacitance in [17] and [18], we propose to use polychronous oscillatory neural networks composed of CMOS ring oscillators and switches to emulate quantum gates. Advantages of ring oscillators include compact area, wider tuning range, and low power. [19]–[21]. By using active oscillators connected to a power supply instead of passive resonators, we overcome the problem of dampened oscillations due to nonzero resistance.

The voltage across the i^{th} oscillator is

$$V_i(t) = A_i \cos(\omega_0 t + \theta_i), \quad (1)$$

where ω_0 is the free-running frequency of the oscillator, A_i is the amplitude, and θ_i is the phase.

We now apply the results of [22], that were originally developed for LC resonators, to our oscillators. An N -qubit state is defined by the superposition of the 2^N states,

$$|\psi\rangle = \sum_{i=0}^{2^N-1} \alpha_i |i\rangle, \quad (2)$$

where i is the integer corresponding to the binary number. For example, in a two-qubit system, $0\rangle = |00\rangle$, $1\rangle = |01\rangle$, $2\rangle = |10\rangle$, and $3\rangle = |11\rangle$. We can express the coefficient in the oscillator realization of quantum computing,

$$\alpha_i = A_i e^{j\theta_i} / \sqrt{\sum_i (A_i)^2}. \quad (3)$$

We design our system of oscillators so there is phase synchronization across oscillators, and the phase of each oscillator is referenced to a common reference phase. To this end, all oscillators are injected with a master pump signal at f_0 , where f_0 is the natural oscillation frequency. Then, we can choose the same node of any oscillator (such as V_4 in Fig 3) and expect the same phase. If we did not have the pump, then the phase of each oscillator is random and not known a priori.

Now, we derive the steady state solution for the oscillatory CNN and solve for the phase between each oscillator and the pump. Each oscillator in the neural network is under injection from the master pump signal at frequency ω_{pump} . We can apply impulse sensitivity function (ISF) theory and the pulling equation for a single oscillator is

$$\frac{d\theta_i}{dt} = \omega_0 - \omega_{\text{pump}} + \frac{1}{T_{\text{pump}}} \int_{T_{\text{pump}}} \tilde{\Gamma}(\omega_{\text{pump}} t + \theta_i) \cdot i_{\text{pump}}(t) dt. \quad (4)$$

This equation determines the steady-state phase of each oscillator in the network. $\tilde{\Gamma}(\omega_0 \tau)$ is the ISF and captures the sensitivity of an oscillator to an injected impulse at phase $\omega_0 \tau$ [23]–[25]. $i_{\text{pump}}(t)$ is the injection current from the master pump. In the steady state, $\frac{d\theta_i}{dt} = 0$. Then, for $\omega_0 = \omega_{\text{pump}}$, the integral evaluates to 0 for a unique value of θ_i . Thus, the oscillator $V_i(t)$ waveforms are in phase if they are injected with a master pump, as will be confirmed by simulations.

III. UNIVERSAL QUANTUM GATES: RING OSCILLATOR IMPLEMENTATION

In this section, we demonstrate how to emulate a set of universal quantum gates using oscillatory cellular neural

networks composed of CMOS ring oscillators and switches. For illustrative purposes, we focus on two-qubit systems with four oscillators.

A. Controlled NOT (CNOT) Gate

The CNOT gate takes two qubits as inputs, where the first qubit is the control qubit. The CNOT gate inverts the target qubit if the control qubit is $|1\rangle$. The CNOT gate matrix is

$$U_{\text{CNOT}} = \begin{bmatrix} 1 & 0 & 0 & 0 \\ 0 & 1 & 0 & 0 \\ 0 & 0 & 0 & 1 \\ 0 & 0 & 1 & 0 \end{bmatrix}. \quad (5)$$

For the 2-qubit system, a qubit in the state $|10\rangle$ becomes $|11\rangle$ after the CNOT gate. Similarly, a qubit in the state $|11\rangle$ becomes $|10\rangle$ after the CNOT gate.

The CNOT gate can be implemented by first checking if control qubit is $|1\rangle$. If so, the output of this comparison drives the CMOS switches of the $|10\rangle$ and $|11\rangle$ oscillators. The switch for the input oscillator state is opened, while the switch for the output oscillator state is turned on.

B. $\frac{\pi}{4}$ Phase Shift Gate

The $\frac{\pi}{4}$ phase shift gate results in a phase shift of 45° when the qubit is in state $|1\rangle$. The $\frac{\pi}{4}$ phase shift gate matrix is

$$U_{\frac{\pi}{4}} = \begin{bmatrix} 1 & 0 \\ 0 & e^{j\frac{\pi}{4}} \end{bmatrix}. \quad (6)$$

The $\frac{\pi}{4}$ phase shift can be implemented using a multiphase ring oscillator. A switch is used to select the desired phase of the multiphase oscillator.

C. Hadamard Gate

The Hadamard gate acts on one qubit and produces a superposition of output states. Compared to the CNOT and $\frac{\pi}{4}$ phase shift gates, this superposition property is unique to the Hadamard gate. The Hadamard gate matrix is

$$U_H = \frac{1}{\sqrt{2}} \begin{bmatrix} 1 & 1 \\ 1 & -1 \end{bmatrix}, \quad (7)$$

$$H|0\rangle = \frac{1}{\sqrt{2}}(|0\rangle + |1\rangle), \quad (8)$$

$$H|1\rangle = \frac{1}{\sqrt{2}}(|0\rangle - |1\rangle). \quad (9)$$

The Hadamard gate can be implemented by turning on the appropriate switch, so two ring oscillators oscillate simultaneously. Then, switches are used to select the oscillator waveform with 0° or 180° phase. Finally, the supply voltages for each oscillator's output buffer are reduced to $\frac{V_{DD}}{\sqrt{2}}$. The Hadamard gate and its polychronous oscillator implementation is shown in Fig. 2.

IV. CIRCUIT DESIGN AND SIMULATION RESULTS

In this section, we present illustrative circuit design and simulation results for an oscillatory CNN machine for quantum gate emulation. The system is designed in 65nm CMOS.

The unit oscillator schematic is shown in Fig. 3 and is adapted from [15]. The oscillator's free running frequency is close to 250 MHz, while the pump signal is a 250 MHz sinusoid with $4 \mu A$ amplitude. The pump signal is injected to

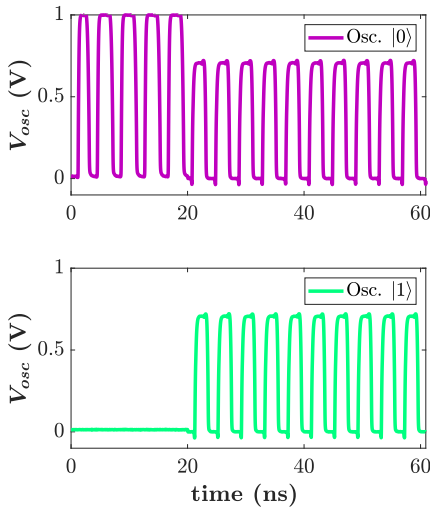


Fig. 2. Hadamard gate's polychronous oscillator implementation. In this example, only the $|0\rangle$ oscillator is oscillating initially. The Hadamard gate produces a superposition of output states. Both the $|1\rangle$ and $|0\rangle$ oscillators now oscillate, with reduced amplitude relative to the initial amplitude of the $|0\rangle$ oscillator.

all oscillators at the V_1 node. V_{reg} is the supply voltage for an oscillator's output buffer. In practice, the V_{reg} voltage levels can be generated from a voltage regulator. By changing the supply voltage of the buffer instead of the oscillator supply voltage, the oscillators' voltage swing and frequency remain fixed across quantum gate operations. This design based on inverters and switches is digital-CMOS friendly and amenable to porting across technology nodes.

A. Greenberger–Horne–Zeilinger (GHZ) State

The first example is the Greenberger–Horne–Zeilinger (GHZ) state, which is an entangled quantum state. The quantum circuit diagram is shown in Fig. 4 and consists of one Hadamard gate and two CNOT gates. In a quantum circuit diagram, the states evolve from left to right. Unlike in an electronic circuit diagram, superposition states are permitted. In our examples, we use little endian notation for the qubits.

The initial state of the quantum circuit is $|000\rangle$. First, the Hadamard gate takes q_0 as an input and the output is the superposition,

$$|H\rangle = \frac{|000\rangle + |001\rangle}{\sqrt{2}}. \quad (10)$$

The CNOT gate inverts the target qubit if the control qubit is $|1\rangle$. Otherwise, the target bit is unchanged. The upper CNOT gate has control qubit q_0 and target qubit q_1 and its output is

$$|CNOT\rangle = \frac{|000\rangle + |011\rangle}{\sqrt{2}}. \quad (11)$$

The lower CNOT gate has control qubit q_1 and target qubit q_2 , and the output of the overall circuit is the GHZ state,

$$|GHZ\rangle = \frac{|000\rangle + |111\rangle}{\sqrt{2}}. \quad (12)$$

Our oscillatory cellular neural network implementation is shown in Fig. 1 and the three qubits are represented by eight oscillators. The system is initialized so $|000\rangle$ has 100%

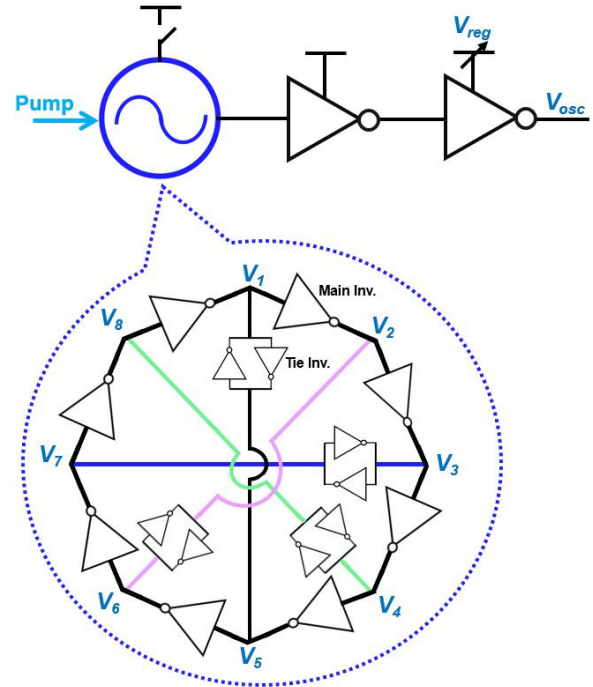


Fig. 3. Schematic of an octahedral oscillator (modified from [15]) with buffer, that represents a quantum state. Switches are used to enable or disable oscillation.

probability. We first close the switch and begin oscillation for the ring oscillator representing $|000\rangle$. This $|000\rangle$ oscillator's buffered output has a voltage swing of V_{DD} . Next, the Hadamard gate acts on q_0 and results in a superposition state. Thus, the switch for $|001\rangle$ oscillator is turned on. The buffer voltages for $|000\rangle$ and $|001\rangle$ oscillators are reduced to $\frac{V_{DD}}{\sqrt{2}}$.

Next, the upper CNOT gate checks if its control bit, q_0 , is $|1\rangle$. Since q_0 is $|1\rangle$ for the $|001\rangle$ state, the target bit is inverted. Thus, the switch for $|001\rangle$ ring oscillator is opened and this oscillator stops oscillating. Then, the switch for $|011\rangle$ oscillator is turned on. The supply voltage of the $|011\rangle$ oscillator's buffer is also $\frac{V_{DD}}{\sqrt{2}}$. Similarly, the lower CNOT gate causes the switch for the $|011\rangle$ ring oscillator to be opened, to stop its oscillation. Finally, the switch for the $|111\rangle$ oscillator is turned on and the supply voltage for this oscillator's buffer is $\frac{V_{DD}}{\sqrt{2}}$. By observing the final state of the eight oscillators, we observe only the $|000\rangle$ and $|111\rangle$ oscillators are oscillating, with equal amplitudes. Thus, the final state has a 50% probability of $|000\rangle$ and 50% probability of $|111\rangle$.

A transient simulation with noise is run using SpectreRF and the oscillatory neural network's buffered outputs from V_{osc} node are shown in Fig. 4(b). Four oscillator waveforms are shown, since the other four oscillators have 0% probability for all time and do not oscillate. To make the oscillator waveforms representing quantum gate operations easier to view, each quantum gate acts for 20 ns. This time can be reduced to reach the final solution faster. We observe the steady state solution around 70 ns, where the $|000\rangle$ and $|111\rangle$ oscillator outputs each oscillate with a swing of 707 mV, compared to $|000\rangle$ oscillator's initial swing of 1 V. The quantum circuit was

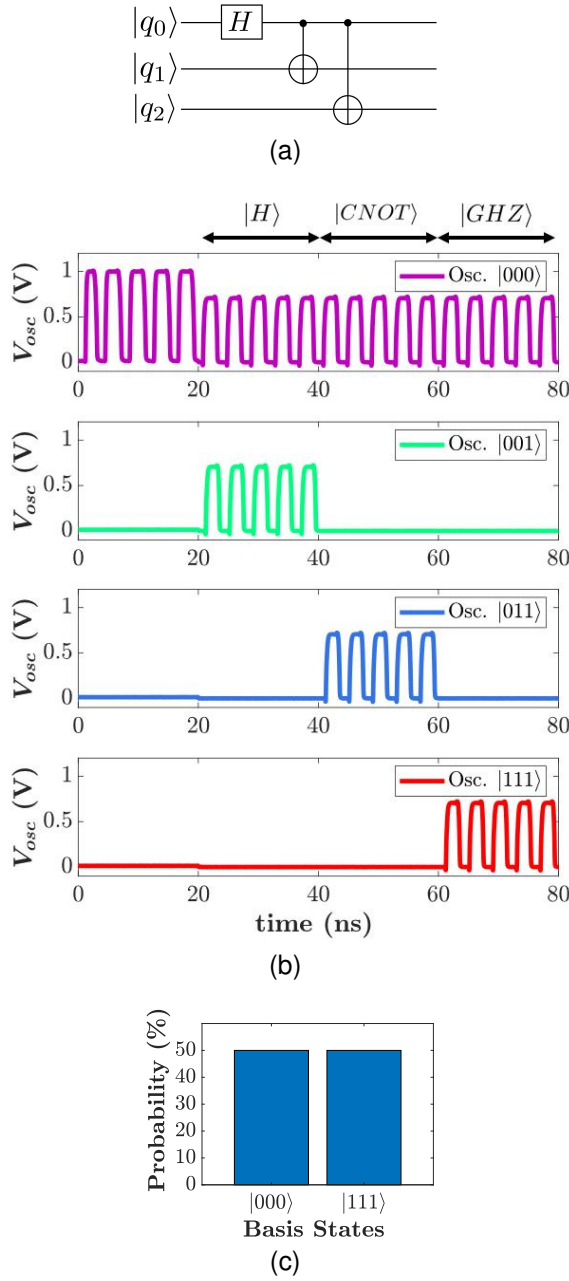


Fig. 4. Simulation results for the Greenberger–Horne–Zeilinger (GHZ) State. (a) Quantum circuit diagram. (b) Spectre simulation results. (c) IBM Quantum Composer simulation results, confirming agreement with (b).

also simulated with IBM Quantum Composer and the result shown in Fig. 4(c) is in agreement with our proposed CMOS oscillator approach.

B. W State

The second example is the W state, which is also an entangled quantum state. The quantum circuit diagram is shown in Fig. 5 and consists of one Ry-rotation gate, one controlled Hadamard gate, two CNOT gates, and one X gate. The input state to the quantum circuit is $|000\rangle$. First, this Ry-rotation gate takes q_0 as an input and rotates around the y-axis by $\theta = 1.91$ radians. This scales the amplitude,

$$|Ry\rangle = \frac{1}{\sqrt{3}} |000\rangle + \sqrt{\frac{2}{3}} |001\rangle. \quad (13)$$

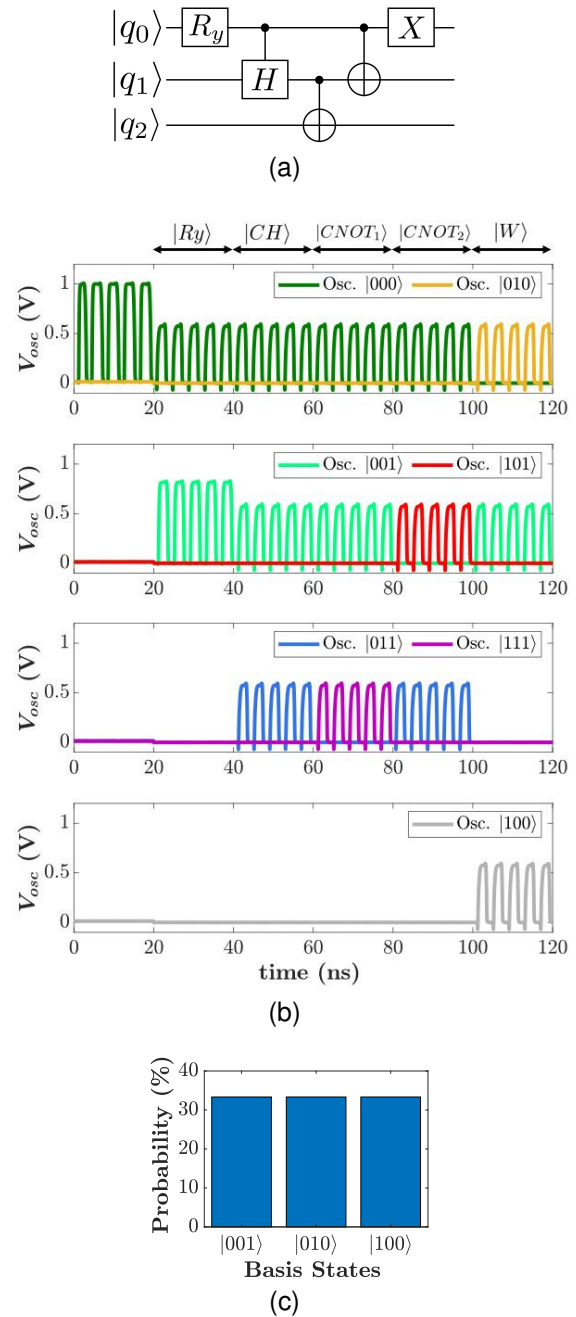


Fig. 5. Simulation results for the W State. (a) Quantum circuit diagram. (b) Spectre simulation results. (c) IBM Quantum Composer simulation results.

The controlled Hadamard gate produces an output superposition if the control qubit is $|1\rangle$. Here, the control qubit is q_0 , while the target qubit is q_1 . The output of the controlled Hadamard gate is

$$|CH\rangle = \frac{1}{\sqrt{3}} (|000\rangle + |001\rangle + |011\rangle). \quad (14)$$

The lower CNOT gate takes control bit q_1 and target bit q_2 ,

$$|CNOT_1\rangle = \frac{1}{\sqrt{3}} (|000\rangle + |001\rangle + |111\rangle). \quad (15)$$

The upper CNOT gate takes control bit q_0 and target bit q_1 ,

$$|CNOT_2\rangle = \frac{1}{\sqrt{3}} (|000\rangle + |011\rangle + |101\rangle). \quad (16)$$

The X gate inverts q_0 and the final output is the W State,

$$|W\rangle = \frac{1}{\sqrt{3}}(|001\rangle + |010\rangle + |100\rangle). \quad (17)$$

In our CMOS circuit implementation, the system is again initialized with $|000\rangle$ at 100% probability. We first close the switch and begin oscillation for the oscillator representing $|000\rangle$. This $|000\rangle$ oscillator has a voltage swing of V_{DD} . Next, the Ry-rotation gate acts on q_0 and results in a superposition state. Thus, the switch for $|001\rangle$ ring oscillator is turned on. The supply voltages for $|000\rangle$ oscillator's buffer is reduced to $\frac{1}{\sqrt{3}}V_{DD}$ and $|001\rangle$ oscillator's buffer is reduced to $\frac{\sqrt{2}}{\sqrt{3}}V_{DD}$.

Next, the controlled Hadamard gate acts on q_1 and results in a superposition state. Thus, the switch for $|011\rangle$ ring oscillator is turned on. The supply voltages for $|001\rangle$ and $|011\rangle$ oscillator buffers are reduced to $\frac{1}{\sqrt{3}}V_{DD}$. Then, the lower CNOT gate checks if its control bit, q_1 , is $|1\rangle$. If q_1 is $|1\rangle$, the target bit is inverted. Thus, the switch for $|011\rangle$ ring oscillator is opened and this oscillator stops oscillating. Next, the switch for $|111\rangle$ ring oscillator is turned on. The supply voltage of the $|111\rangle$ oscillator's buffer is also $\frac{1}{\sqrt{3}}V_{DD}$.

Similarly, the upper CNOT gate causes the switch for the $|001\rangle$ and $|111\rangle$ ring oscillators to be opened. Then the switches for the $|011\rangle$ and $|101\rangle$ ring oscillators are turned on and their buffers' supply voltages are reduced to $\frac{1}{\sqrt{3}}V_{DD}$. Finally, the X gate causes the switch for the $|011\rangle$ and $|101\rangle$ ring oscillators to be opened. Lastly, the switches for the $|010\rangle$ and $|001\rangle$ ring oscillators are turned on and their buffers' supply voltages are $\frac{1}{\sqrt{3}}V_{DD}$. By observing the final state of the eight oscillators, we observe the $|001\rangle$, $|010\rangle$, and $|100\rangle$ oscillators are oscillating, with equal amplitudes. Thus, the final state has a 33% probability of $|001\rangle$ state, 33% probability of $|010\rangle$ state, and 33% probability of $|100\rangle$ state.

Spectre simulation results of the oscillatory neural network's buffered outputs from V_{osc} node are shown in Fig. 5(b). Seven oscillator waveforms are shown, since the $|110\rangle$ oscillator has 0% probability for all time and does not oscillate. We observe the steady state solution around 110 ns, where the $|001\rangle$, $|010\rangle$, and $|100\rangle$ oscillator outputs each oscillate with a swing of 577 mV, compared to $|000\rangle$ oscillator's initial swing of 1 V. The quantum circuit was also simulated with IBM Quantum Composer and the result shown in Fig. 5(c) is in agreement with the Spectre CMOS circuit simulation.

V. CONCLUSION

We have proposed quantum computing gate emulation using polychronous oscillatory cellular neural networks. We demonstrated how to emulate universal quantum gates using an oscillatory cellular neural network with CMOS ring oscillators and switches. We have used impulse sensitivity function (ISF) theory to model the injection locking of the oscillatory cellular neural network. We present CMOS circuit design examples and design guidelines. Spectre simulations confirm the polychronous oscillatory cellular neural network can emulate quantum circuits, such as the Greenberger–Horne–Zeilinger State and W State. This architecture can be scaled up and extended to emulate other quantum circuits and algorithms.

REFERENCES

- [1] C. Mead, *Analog VLSI and Neural Systems*. Boston, MA: Addison-Wesley, 1989.
- [2] B. V. Benjamin, R. L. Smith, and K. A. Boahen, "An analytical MOS device model with mismatch and temperature variation for subthreshold circuits," *IEEE Trans. Circuits Syst. II, Exp. Briefs*, vol. 70, no. 6, pp. 1826–1830, 2023.
- [3] A. Neckar, S. Fok, B. V. Benjamin, T. C. Stewart, N. N. Oza, A. R. Voelker, C. Eliasmith, R. Manohar, and K. Boahen, "Braindrop: A mixed-signal neuromorphic architecture with a dynamical systems-based programming model," *Proc. IEEE*, vol. 107, no. 1, pp. 144–164, 2019.
- [4] P. Boriskov, "Chaotic LIF oscillator with variable resistance feedback and nonlinear rate coding," *IEEE Transactions on Circuits and Systems II: Express Briefs*, vol. 69, no. 6, pp. 2982–2986, 2022.
- [5] R. P. Feynman, "Simulating physics with computers," *Int. J. Theor. Phys.*, vol. 21, no. 6, pp. 467–488, Jun 1982.
- [6] E. Rieffel and W. Polak, *Quantum Computing: A Gentle Introduction*, 1st ed. The MIT Press, 2011.
- [7] M. A. Nielsen and I. L. Chuang, *Quantum Computation and Quantum Information*. Cambridge University Press, 2000.
- [8] P. Kaye, R. Laflamme, and M. Mosca, *An Introduction to Quantum Computing*. New York: Oxford University Press, Inc., 2007.
- [9] Semiconductor Research Corporation and Semiconductor Industry Association, "Rebooting the IT revolution: A call to action," Semiconductor Research Corporation, Tech. Rep., 2015.
- [10] F. Ware, L. Gopalakrishnan, E. Linstadt, S. A. McKee, T. Vogelsang, K. L. Wright, C. Hampel, and G. Bronner, "Do superconducting processors really need cryogenic memories? The case for cold DRAM," in *Proc. Int. Symp. on Memory Systems*, New York, 2017, p. 183–188.
- [11] D. Marković and J. Grollier, "Quantum neuromorphic computing," *Applied Physics Letters*, vol. 117, no. 15, p. 150501, 10 2020.
- [12] L. Chua and L. Yang, "Cellular neural networks: theory," *IEEE Trans. Circuits and Systems*, vol. 35, no. 10, pp. 1257–1272, 1988.
- [13] G. Manganaro, "Another look at cellular neural networks," in *Int. Workshop on Cellular Nanoscale Networks and their Applications (CNNA)*, 2021, pp. 1–4.
- [14] A. Ascoli, R. Tetzlaff, S.-M. Kang, and L. O. Chua, "Theoretical foundations of memristor cellular nonlinear networks: A DRM2-based method to design memcomputers with dynamic memristors," *IEEE Trans. Circuits Syst. I, Reg. Papers*, vol. 67, no. 8, pp. 2753–2766, 2020.
- [15] R. L. Smith and T. H. Lee, "Polychronous oscillatory cellular neural networks for solving graph coloring problems," *IEEE Open Journal of Circuits and Systems*, vol. 4, pp. 156–164, 2023.
- [16] G. Csaba and W. Porod, "Coupled oscillators for computing: A review and perspective," *Appl. Phys. Rev.*, vol. 7, no. 1, p. 011302, Jan. 2020.
- [17] M. Ezawa, "Universal quantum gates, artificial neurons, and pattern recognition simulated by LC resonators," *Phys. Rev. Res.*, vol. 3, p. 023051, Apr 2021.
- [18] M. M. Islam, S. Hossain, and A. Aziz, "A SPICE-based framework to emulate quantum circuits with classical LC resonators," in *Int. Symp. on Quality Electronic Design (ISQED)*, 2023, pp. 1–7.
- [19] R. L. Smith and T. H. Lee, "Analysis and design of a tetrahedral oscillator," *IEEE Trans. Circuits Syst. II: Express Br.*, vol. 69, no. 1, pp. 75–79, 2022.
- [20] J. Arenas, J. S. Moya, and E. Roa, "A 15000 tuning range scalable feed-forward oscillator with 0.05mm² area in CMOS standard-cell format," in *IEEE Int. Symp. on Circuits and Systems (ISCAS)*, 2021, pp. 1–4.
- [21] S. M. Schober and J. Choma, "A capacitively phase-coupled low noise, low power 0.8-to-28.2 GHz quadrature ring VCO in 40nm CMOS," in *IEEE Int. New Circuits and Systems Conference (NEWCAS)*, 2015, pp. 1–4.
- [22] M. Ezawa, "Non-Abelian braiding of Majorana-like edge states and topological quantum computations in electric circuits," *Phys. Rev. B*, vol. 102, p. 075424, Aug 2020.
- [23] A. Hajimiri and T. H. Lee, "A general theory of phase noise in electrical oscillators," *IEEE J. Solid-State Circuits*, vol. 33, no. 2, pp. 179–194, 1998.
- [24] B. Hong and A. Hajimiri, "A general theory of injection locking and pulling in electrical oscillators—part I: Time-synchronous modeling and injection waveform design," *IEEE J. Solid-State Circuits*, vol. 54, no. 8, pp. 2109–2121, 2019.
- [25] —, "A general theory of injection locking and pulling in electrical oscillators—part II: Amplitude modulation in LC oscillators, transient behavior, and frequency division," *IEEE J. Solid-State Circuits*, vol. 54, no. 8, pp. 2122–2139, 2019.